387

An integrated model for pore pressure accumulations in marine sediment under combined wave and current loading

Y. Zhang [1a], D.-S. Jeng [*1,2], H.-Y. Zhao [2b] and J.-S. Zhang [3c]

[1] *Department of Civil Engineering, State Key Laboratory of Ocean Engineering,*
Shanghai Jiao Tong University, Shanghai 200240, China
[2] *Griffith School of Engineering, Griffith University Gold Coast Campus, Queensland, QLD 4222, Australia*
[3] *State Key Laboratory of Hydrology-Water Resources and Hydraulic Engineering,*
Hohai University, Nanjing, Jiangsu 210098, China

Abstract. In this paper, an integrated model for the wave (current)-induced seabed response is presented. The present model consists of two parts: hydrodynamic model for wave-current interactions and poro-elastic seabed model for pore accumulations. In the wave-current model, based on the fifth-order wave theory, ocean waves were generated by adding a source function into the mass conservation equation. Then, currents were simulated through imposing a steady inlet velocity on one domain and pressure outlet on the other side. In addition, both of the Reynolds-Averaged Navier-Stokers (RANS) Equations and *k-ε* turbulence model would be applied in the fluid field. Once the wave pressures on the seabed calculated through the wave-current interaction model, it would be applied to be boundary conditions on the seabed model. In the seabed model, the poro-elastic theory would be imposed to simulate the seabed soil response. After comparing with the experimental data, the effect of currents on the seabed response would be examined by emphasize on the residual mechanisms of the pore pressure inside the soil. The build-up of the pore water pressure and the resulted liquefaction phenomenon will be fully investigated. A parametric study will also be conducted to examine the effects of waves and currents as well as soil properties on the pore pressure accumulation.

Keywords: waves and currents; poro-elastic; pore pressure accumulation; liquefaction

1. Introduction

The phenomenon of wave-seabed interactions has attracted great attentions among coastal and geotechnical engineers in the last three decades. Among these, seabed stability is one of the key factors to be considered in the design of offshore structures (e.g., breakwaters, pipelines, oil production platforms). One main reason that causes the instability of these offshore structures is the increase of the excess pore pressure in the soil which would possibly lead to the water-sediment mixture acting like a liquid when the excess pore pressure increases to a certain level.

∗Corresponding author, Ph.D., Professor, E-mail: d.jeng@griffith.edu.au
[a] Ph.D. Student, E-mail: zhangyu05200308@sjtu.edu.cn
[b] Ph.D. Student, E-mail: hongyi.zhao@griffithuni.edu.au
[c] Ph.D., Professor, E-mail: jszhang@hhu.edu.cn

Therefore it is necessary to give a precise prediction of the excess pore pressure and liquefaction in a porous seabed during the design of marine infrastructures.

It has been well known that currents and waves exist simultaneously in real marine environments, and current plays an important role on the transportation and scouring above the seabed surface. Many works have been done regarding the phenomenon of wave-current interactions (Grant and Madsen 1979, Kemp and Simons 1982, 1983, You 1994, Hsu *et al.* 2009, Umeyama 2009). Among these, the most widely developed numerical model to simulate wave-current interaction is based on Navier Stokers equations, which directly provide the solutions describing wave pattern and current state simultaneously. Park *et al.* (2001) proposed a numerical wave tank simulation with a finite-difference scheme and a marker-and-cell method to investigate wave motions and their interactions with steady uniform currents. Li *et al.* (2007) proposed a NS solver as well as volume of fluid (VOF) method and SGS turbulence model to simulate the interactions between breaking waves and a current over a cut-cell grid. Markus *et al.* (2013) applied a CFD solver to simulate the flow field of a nonlinear wave with a non-uniform current.

When waves and currents propagated over the ocean surface, they exert dynamic pressures on the seabed sediment grains, which contribute to the changes of the pore pressures within the soil skeleton. Generally speaking, the mechanism of pore pressure changing can be divided into two categories (Zen and Yamazaki 1990). One is oscillatory excess pore pressure with periodical response to waves, companied by amplitude damping and phase lag in pore pressure (Yamamoto *et al.* 1978). The liquefaction of this mechanism generally occurs during the passage of the wave trough, which imposes an upward lift force on the soil grains. When the lift force reaches the submerged weight of the soil, liquefaction would occur. This phenomenon usually happens in an unsaturated soil and lasts only for few seconds. The other one is residual pore pressure, which appears at the initial stage of the cyclic loading (Seed and Rahman 1978). Under this mechanism, the process of residual excess pore pressure's builds up comes to an end until the effective stress between the individual grains vanishes, then the seabed soil acts like a fluid and liquefaction occurs. In this study, we emphasize on the residual liquefaction.

To get a better understanding of the above problems, it is obvious that simple elastic models for the seabed could not reveal the real soil characteristics, especially encountered with the build-up phenomenon of pore pressure among seabed soil grains. There has existing a lot of works, which found that the cyclic shear stress ratio is one of the most important factors in the pore water pressure accumulation process. As pointed out by Seed and Lee (1966), the magnitude of cyclic stresses has influence on the build-up process of pore pressures. Seed and Rahman (1978) then studied the cyclic plasticity of soils under progressive waves and took into account the distribution of the cyclic shear stress in the soil profile as well as the important factor of pore pressure dissipation. By adopting the same assumptions proposed by Seed and Rahman (1978), Sumer and Cheng (1999), Jeng and Seymour (2007) further analytically investigated the pore pressure accumulation, respectively. Sekiguchi *et al.* (1995) derived a one-dimensional closed-form poro-elastoplastic solution for the cumulative contraction of soils under cyclic loading of standing waves. In addition to theoretical approaches, several series of experiments with respect to wave-induced pore pressure build up has been conducted. Among these, Sekiguchi *et al.* (1995), Sassa and Sekiguchi (1999) presented a series of experimental results for the wave-induced residual pore pressure from centrifuge wave tank tests. Recently, Sumer *et al.* (2012) conducted an experimental study to find how pore pressures build up by taking into account both liquefaction and no-liquefaction situations.

Recently, a few investigations for the wave (current)-induced soil response in a porous seabed

have been carried out. All of them have focus on the oscillatory pore pressures, rather than residual pore pressures and their approaches have been based on poro-elastic models (Ye and Jeng 2012, Zhang *et al*. 2013a, b, Liu *et al*. 2014, Liao *et al*. 2015). In addition to theoretical studies, some experiments in wave flumes have been reported (Qi and Gao 2014).

In this paper, a numerical wave-current model would be presented on the basis of RANS equations and *k-ε* turbulence model. Then, a two-dimensional poro-elastic model, which focuses on the accumulation of pore water pressure, would be conducted. After validation of the present seabed model, the seabed response due to combined waves and currents would be investigated. A parametric study would be carried out to investigate the effects of currents and soil characteristics on seabed response. Then, the liquefaction analysis would be conducted under the liquefaction criterion, which supplies a good visualized demonstration of the stability of seabed.

2. Theoretical formulations

In the present study, an internal wave-maker model is added beneath the ocean surface to generate 5th order progressive waves. The Reynolds-Averaged Navier-Stokes (RANS) solver, with finite-volume scheme, VOF method and *k-ε* turbulent model will be developed here to simulate waves and currents flow fields. With the solutions of the dynamic fluid pressures and shear stresses obtained from the wave-current model, the boundary condition of the seabed could be settled down. The present two-dimensional poro-elastic seabed model has a time-dependent feature, which is different with the previous models. Based on the integrated model, the seabed responses could be studied effectively.

2.1 Wave-current model

The incompressible fluid motion could be described by RANS Equations that consist of mass conservation equation and momentum conservation equation

$$\frac{\partial \langle u_i \rangle}{\partial x_i} = 0 \tag{1}$$

$$\frac{\partial \rho_f \langle u_i \rangle}{\partial t} + \frac{\partial \rho_f \langle u_i \rangle \langle u_j \rangle}{\partial x_j} = -\frac{\partial \langle p \rangle}{\partial x_i} + \frac{\partial}{\partial x_j}\left[\mu\left(\frac{\partial \langle u_i \rangle}{\partial x_j} + \frac{\partial \langle u_j \rangle}{\partial x_i}\right)\right] + \frac{\partial}{\partial x_j}\left(-\rho_f \langle u_i' u_j' \rangle\right) + \rho_f g_i \tag{2}$$

where x_i is the Cartesian coordinate, $\langle u_i \rangle$ is ensemble mean velocity component, ρ_f is fluid density, t is time, $\langle p_i \rangle$ is fluid pressure, μ is dynamic viscosity, and g is acceleration due to gravity. The Reynolds stress term $-\rho_f \langle u_i' u_j' \rangle$ could be written in the following form by applying eddy-viscosity assumption

$$-\rho_f \langle u_i' u_j' \rangle = \mu_t \left[\frac{\partial \langle u_i \rangle}{\partial x_j} + \frac{\partial \langle u_j \rangle}{\partial x_i}\right] - \frac{2}{3}\rho_f \delta_{ij} k \tag{3}$$

where μ_t is the turbulent viscosity, k is turbulence kinetic energy (TKE) and δ_{ij} is Kronecker delta.

Substituting Eq. (3) to Eq. (2) yields

$$\frac{\partial \rho_f \langle u_i \rangle}{\partial t} + \frac{\partial \rho_f \langle u_i \rangle \langle u_j \rangle}{\partial x_j} = -\frac{\partial}{\partial x_i}\left[\langle p \rangle + \frac{2}{3}\rho_f k\right] + \frac{\partial}{\partial x_j}\left[\mu_{eff}\left(\frac{\partial \langle u_i \rangle}{\partial x_j} + \frac{\partial \langle u_j \rangle}{\partial x_i}\right)\right] + \rho_f g_i \tag{4}$$

in which $\mu_{eff} = \mu + \mu_t$ is the total effective viscosity.

For the *k-ε* turbulence model, it has been successfully applied to predict many complex turbulent flows, which could be expressed as (Launder and Spalding 1974)

$$\frac{\partial \rho_f \kappa}{\partial t} + \frac{\partial \rho_f \langle u_j \rangle \kappa}{\partial x_j} = \frac{\partial}{\partial x_j}\left[\left(\mu + \frac{\mu_t}{\sigma_\kappa}\right)\frac{\partial \kappa}{\partial x_j}\right] + \rho_f P_\kappa - \rho_f \varepsilon \tag{5}$$

$$\frac{\partial \rho_f \varepsilon}{\partial t} + \frac{\partial \rho_f \langle u_j \rangle \varepsilon}{\partial x_j} = \frac{\partial}{\partial x_j}\left[\left(\mu + \frac{\mu_t}{\sigma_\varepsilon}\right)\frac{\partial \varepsilon}{\partial x_j}\right] + \frac{\varepsilon}{\kappa}(C_{\varepsilon 1}\rho P_\kappa - C_{\varepsilon 2}\rho\varepsilon) \tag{6}$$

$$\mu_t = \rho C_\mu \frac{\kappa^2}{\varepsilon} \tag{7}$$

in which κ is the turbulent kinetic energy and ε is the turbulent dissipation rate. The empirical coefficients used in the model are recommended as (Rodi 1993)

$$C_\mu = 0.09, \quad C_{\varepsilon 1} = 1.44, \quad C_{\varepsilon 2} = 1.92, \quad \sigma_\kappa = 1.00, \quad \sigma_\varepsilon = 1.30 \tag{0}$$

In the wave-current model, waves are generated through the internal wave-maker model (Lin and Liu 1999). A source function $S(x_i, t)$ was added to the mass conservation equation which could be written as

$$\frac{\partial \langle u_i \rangle}{\partial x_i} = S(x_i, t) \tag{8}$$

For the fifth-order Stokes wave applied in this study, the source term is given as

$$S(x_i, t) = \sum_{j=1}^{5} \frac{2C}{A} a_j \cos j(\frac{\pi}{2} - \omega t - p_s) \tag{9}$$

where A is the area of the source region, C is the wave celerity, a_j is the wave amplitude, ω is the wave frequency, p_s is the phase shift constant. To get a better result, the source region is suggested to be chosen as a rectangle, which has a height of 1/10 of water depth varying between $0.65d$ and $0.75d$ and a width of 1/20 of the wavelength.

2.2 Poro-elastic seabed model

In the poro-elastic seabed model, the wave induced pore pressure could be divided into two components: oscillatory pore pressure and residual pore pressure

$$u_e = u_{e1} + u_{e2} \tag{10}$$

where u_e is the wave induced excess pore pressure at a fixed position, u_{e1} represents the oscillatory component, and u_{e2} denotes the residual component. In the following subsections, both of the two parts would be studied respectively.

2.2.1 Oscillatory soil response

Based on Biot's consolidation theory (Biot 1941), the governing equation for the poro-elastic soil could be described as

$$G\nabla^2 u_s + \frac{G}{(1-2\mu_s)}\frac{\partial}{\partial x}(\frac{\partial u_s}{\partial x} + \frac{\partial w_s}{\partial z}) = -\frac{\partial u_{e1}}{\partial x} \tag{11}$$

$$G\nabla^2 w_s + \frac{G}{(1-2\mu_s)}\frac{\partial}{\partial z}(\frac{\partial u_s}{\partial x} + \frac{\partial w_s}{\partial z}) = -\frac{\partial u_{e1}}{\partial z} \tag{12}$$

where G is the shear modulus of seabed soil; (u_s, w_s) are the soil displacements in the x- and z-directions, respectively; μ_s is Poisson's ratio.

Considering the seabed as hydraulically isotropic with the same permeability K in all directions, the conservation of mass (Biot 1956) leads to

$$\nabla^2 u_{e1} - \frac{\gamma_w n_s \beta_s}{K}\frac{\partial u_{e1}}{\partial t} = \frac{\gamma_w}{K}\frac{\partial \varepsilon}{\partial t} \tag{13}$$

where γ_w is the unit weight of pore water; n_s is the soil porosity; the compressibility of pore fluid β_s and the elastic volume strain of soil matrix ε could be defined as

$$\beta_s = \frac{1}{K_w} + \frac{1-S}{P_{w0}} \tag{14}$$

$$\varepsilon = \frac{\partial u_s}{\partial x} + \frac{\partial w_s}{\partial z} \tag{15}$$

in which K_w is the true modulus of elasticity of water (taken as 2×10^9 N/m^2), S is the degree of saturation and P_{w0} is the absolute water pressure.

2.2.1 Residual soil response

The one-dimensional poro-elastic seabed model has been well established by Sumer and Fredøse (2002) and Jeng (2013), which could be expressed as following form

$$\frac{\partial \overline{u}_{e2}}{\partial t} = c_v \frac{\partial^2 \overline{u}_{e2}}{\partial z^2} + f \tag{16}$$

in which $\overline{u}_{e2}$ is the period-averaged wave induced residual pore pressure, c_v is termed as the coefficient of consolidation on the basis of plain-strain assumption and f is the source term which

should be a function of both space and time. Considering that the present study emphasize on the two dimensional problem, Eq. (16) should be rewritten as

$$\frac{\partial \overline{u}_{e2}}{\partial t} = c_v \left(\frac{\partial^2 \overline{u}_{e2}}{\partial x^2} + \frac{\partial^2 \overline{u}_{e2}}{\partial z^2} \right) + f(x,z,t) \tag{17}$$

in which c_v and $f(x,z,t)$ can be expressed as

$$c_v = \frac{GK}{\gamma_w (1 - 2\mu)} \tag{18}$$

$$f(x,z,t) = \frac{\partial u_g}{\partial t} = \frac{\sigma_0'}{T} \left[\frac{|\tau_{ins}(x,z,t)|}{\alpha_r \sigma_0'} \right]^{\frac{1}{\beta_r}} \tag{19}$$

where u_g is the generation of pore water pressure (Seed and Rahman 1978), $\tau_{ins}(x,z,t)$ is the instant oscillatory shear stress, T is the wave period, α_r and β_r are two empirical constants which can be adopted as (Sumer *et al*. 2012)

$$\alpha_r = 0.34 D_r + 0.084 \ , \quad \beta_r = 0.37 D_r - 0.46 \tag{20}$$

the term of $\tau_{ins}(x,z,t)/\sigma_o'$ represents the induced cyclic shear stress ratio which decides the pore pressure accumulation rates, and σ_o' is the initial effective stress, which can be taken as

$$\sigma_0' = \gamma' z \frac{1 + 2K_0}{3} \tag{21}$$

in which γ' is the submerged specific weight of the soil, K_0 is the coefficient of lateral earth pressure.

In the expression of $f(x,z,t)$, the expression of the term $\tau_{ins}(x,z,t)$ is different with former studies which is defined as the amplitude of the shear stress over a wave period. In the present study, the term $\tau_{ins}(x,z,t)$ stands for instant shear stress which is obtained from the result of oscillatory model by solving Biot's consolidation equations (Eqs. (11)-(13)). It clearly reveals the two-dimensional characteristic as well as the time dependent feature in the process of pore pressure accumulation. In addition, by using the new definition of cyclic shear stress, the oscillatory and residual mechanism of pore pressure generation can be well linked together.

It is noted that the present seabed model doesn't consider the dissipation of the pore pressure that requires additional elasto-plastic models. For example, a simple poro-elasto-plastic model proposed by Sassa and Sekiguchi (1999), which was further extended to 2-D (Liao *et al*. 2014) or complicated poro-elasto-plastic model (Jeng and Ou 2010, Ye *et al*. 2013, 2014)

2.3 Boundary conditions

To solve the governing equations of wave-current model and poro-elastic seabed soil model, appropriate boundary conditions are required. The integrated model can be illustrated in Fig. 1, the water depth is d_w, a steady current flow with a velocity of u_o is first achieved across the whole fluid domain, then the desired waves are generated with wave height H and wave period T.
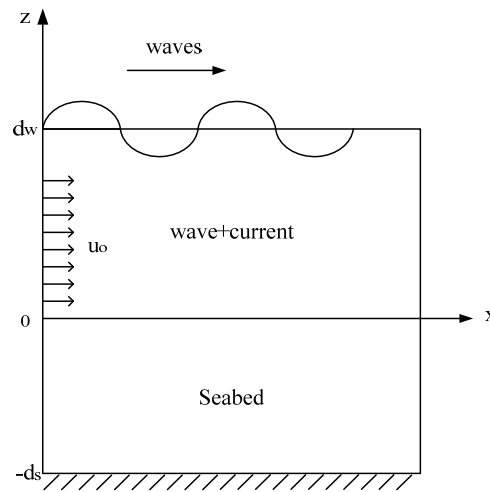
Fig. 1 Problem definition for the system

Here, zero surface tension with $\partial k / \partial \vec{n} = \partial \varepsilon / \partial \vec{n} = 0$ is imposed on the air-water interface, and no-slip boundary is given on the solid surface. Besides, a uniform velocity is provided at the left-hand-side inflow boundary and a pressure outlet is given at the right-hand-side. The whole domain of the wave-current model can be calculated to get the fluid surface elevation, velocity field as well as the water pressure field. The wave pressure along the bottom of the fluid field can be extracted to be boundary condition of seabed soil model, since in the seabed soil model, the pore pressure and the shear stress is equal to the pressure and stress obtained from the wave-current model. The left-hand-side and right-hand-side boundaries of the seabed are considered to be zero-displacement since it is assumed far away from the concerned region. The bottom of the seabed is considered to be impermeable and rigid, and no displacement and vertical flow occur at this boundary.

3. Model validation

The wave-current model could be validated through a comparison between the present study and the experiment result from Qi and Gao (2014). The experiment was conducted in a flow flume which could generate waves and currents simultaneously with 52 m long, 1 m wide and 1.5 m high at the Institute of Mechanics, Chinese Academy of Sciences. A specially designed soil-box is located in the middle section of the flume, and the segment of 2.0 m × 0.5 m × 1.0 m (length × depth × width) is employed in the experiment. Detailed information about the experiment could be found in Qi and Gao (2014).

The parameters of waves and currents Qi and Gao (2014) used in their experiment are listed in Table 1. With these parameters, the numerical study results are compared with the pore pressure measured by PPT1 and PPT2 in that experiment. Figs. 2(a) and (b) illustrate the pore pressures on the seabed surface and beneath the seabed surface in one period, respectively. It could be seen from Fig. 2 that a good agreement existed between the simulated results and laboratory measurement which demonstrate the capacity of the present model in predicting the fluid motion when considering both of the waves and currents.

Table 1 Parameters used in Qi and Gao (2014)'s experiment

		Value	Unit
Wave parameters	Wave height (H)	0.102	[m]
	Wave period (T)	1.2	[s]
	Current velocity (u_o)	0.23	[m/s]
Soil parameters	Soil permeability (K)	$1.88*10^{-4}$	[m/s]
	Relative density (Dr)	0.352	-
	Buoyant unit weight of soil (γ')	9.03	[kN/m^3]

(a) $z = 0$ m   (b) $z = -0.04$ m
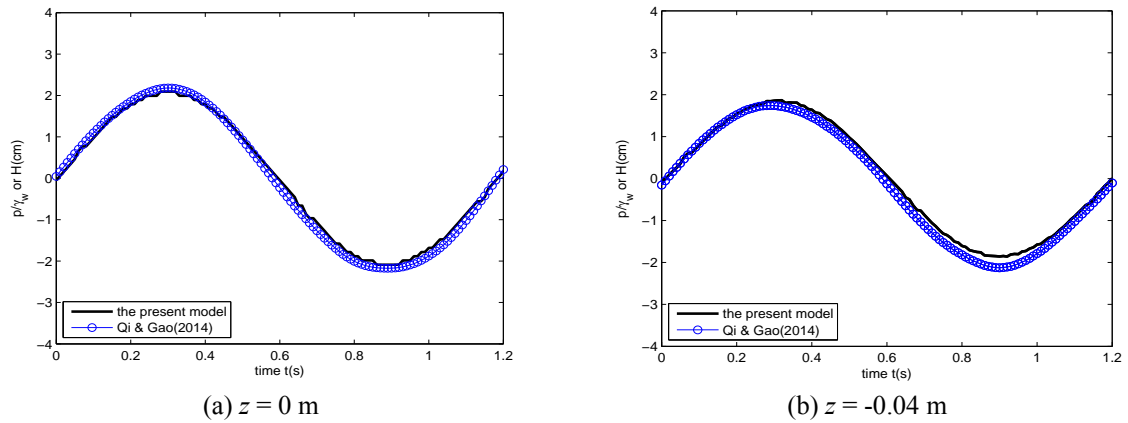
Fig. 2 Comparison of simulated and measured pore pressure on (a) and bellow (b) the seabed surface

Table 2 Parameters used in the comparison with Sassa *et al*. (2001)'s model

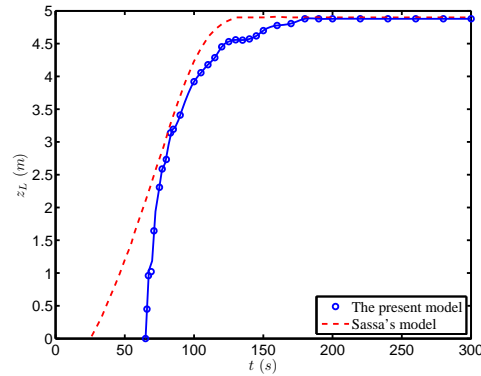|		Value	Unit
Wave parameters	Wave height (H)	6.5	[m]
	Wave period (T)	10	[s]
	Water depth (d_w)	20	[m]
Soil parameters	Seabed Thickness (h)	6	[m]
	Soil permeability (K)	1.5×10^{-4}	[m/s]
	Relative density (Dr)	0.27	-
	Buoyant unit weight of soil (γ')	10.73	[kN/m^3]
	Shear Modulus (G)	5.0×10^6	[N/m2]
	Degree of Saturation (S)	1	-
	Soil porosity (n_s)	0.425	-
	Poisson's ratio (μ_s)	0.35	-
	Coefficient of lateral earth pressure (K_0)	0.41	-

Fig. 3 Comparison of present model and the model of Sassa *et al*. (2001)

Since the present pore-elastic model is developed to study the instability of seabed, the model is compared with a more complex model proposed by Sassa *et al*. (2001). Detailed data used in the comparison are listed in Table 2. It could be seen from Fig. 3 that although there are few differences exist during the maximum liquefaction depth developed process, the final liquefaction depth of the present model is almost the same with the result from Sassa *et al*. (2001), which means this model could give a precise predict of the liquefaction phenomenon in the marine environment.

4. Results and discussions

4.1 Effect of current velocities on wave profiles and seabed response

In this section, the current velocity (u_o) are set variously from -1 m/s to 1 m/s with an interval of 0.5 m/s to explore the effect of current velocity on the wave height and wave length as well as seabed response. Here $u_o = 0$ stands for the case where no current exists, while $u_o \leq 0$ represents when waves travel against the current and $u_o \geq 0$ represents when waves travel following the current. The input data used here are list in Table 3. It can be seen from Fig. 4(a) that when waves travelling with following currents, the wave height become smaller from wave action conservation (defined as wave energy divided by intrinsic angular frequency). On the other hand, it is shown from Fig. 4(b) that when the wave travelling following the current, it results in an increase in wave lengths. That's due to the Doppler shift – the effect of a steady current on intrinsic wave frequency (Wolf and Prandle 1999).

The effect of current velocity on the seabed soil response is also examined here. It is noted that liquefaction occurs when $u_{e2}/\sigma'_{vo} = 1$ and what we focus on is the location near the seabed surface where liquefaction is more likely to occur. As shown in Fig. 5, it is obvious that the current velocity has a great influence on the distribution of accumulated pore pressures. At a given time $t/T = 25$, the seabed in the case of $u_o = $ -1 m/s has already liquefied, while the case $u_o = 0$ m/s just reached its liquefaction status. No liquefaction appears in the case of $u_o = 1$ m/s. It implies that waves with opposite currents reach its liquefaction status faster than waves with following currents, and the case of no current falls in between.

Table 3 Input data for numerical study

		Value	Unit
Wave parameters	Wave height (H)	2	[m]
	Wave period (T)	5	[s]
	Water depth (d_w)	7.8	[m]
Soil parameters	Seabed Thickness (h)	30	[m]
	Soil permeability (K)	1.0×10^{-5}	[m/s]
	Relative density (Dr)	0.3	-
	Shear Modulus (G)	5.0×10^{6}	[N/m^2]
	Degree of Saturation (S)	1	-
	Soil porosity (n_s)	0.425	-
	Poisson's ratio (μ_s)	0.35	-

(a) Wave height   (b) Wave length
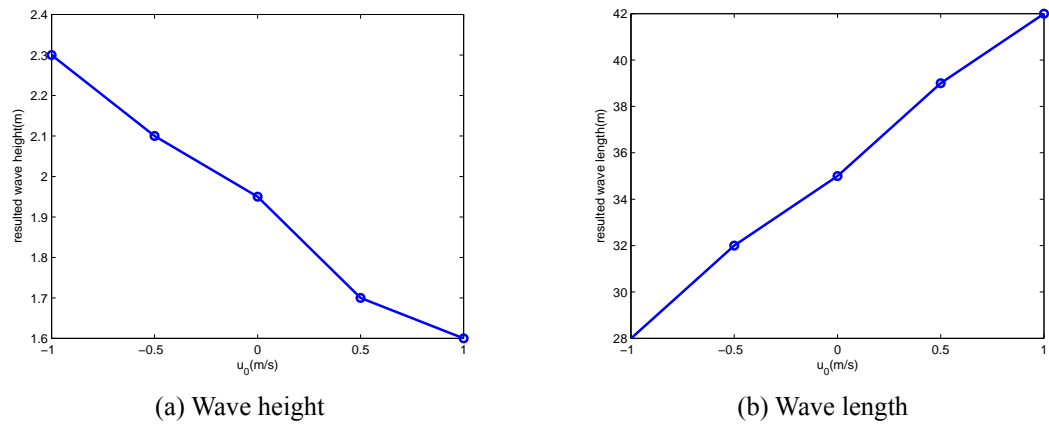
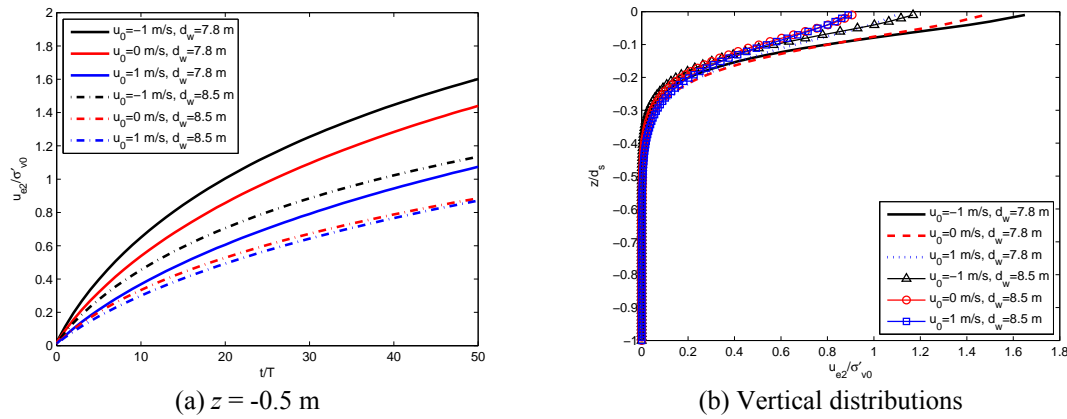Fig. 4 Effect of current velocity on resulted (a) wave height and (b) wave length
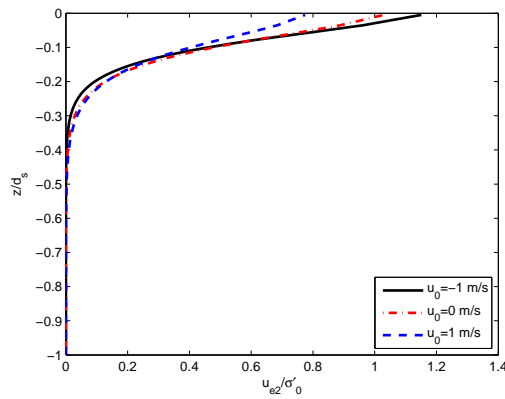
Fig. 5 Effect of current velocity on soil response along z-direction after 25 wave periods

(a) z = -0.5 m

(b) Vertical distributions
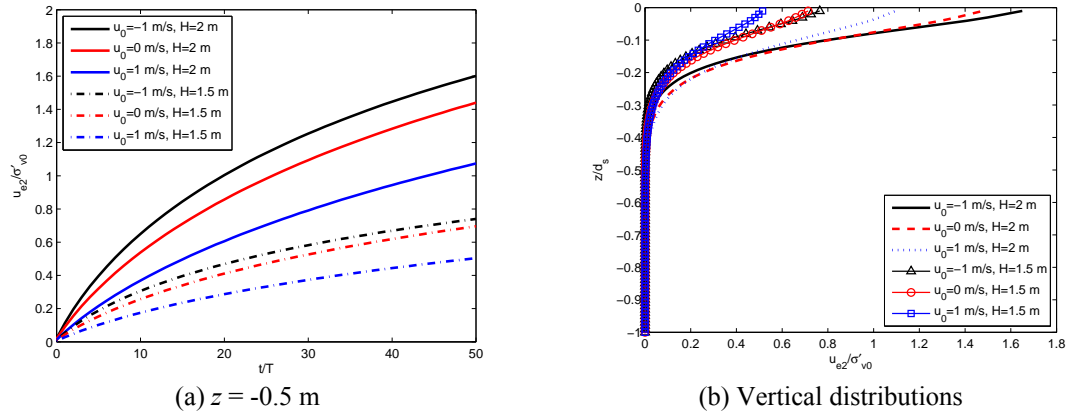
Fig. 6 Pore pressure accumulation with various current velocities and wave heights at t/T = 50

(a) z = -0.5 m

(b) Vertical distributions

Fig. 7 Pore pressure accumulation with various current velocities and water depths at t/T = 50

4.2 Effect of wave properties on seabed response

In this section, the effects of two important wave characteristics (wave height and water depth) on the seabed response would be examined. Fig. 6 (a) shows the build-up process of pore water pressure considering various wave heights and current velocities during 50 wave periods at the depth of z = -0.5 m. The figure shows that higher wave height leads to easier accumulation of the pore pressure and the waves with opposite currents build up faster than the wave alone and the waves with following currents under the same wave condition. This can be further found in Fig. 6 (b) that higher wave height and opposite direction between waves and currents make the soil easy to reach liquefaction. Similar results can be obtained in Fig. 7, which illustrates the effects of current velocity and water depth on the seabed response. From the figure it can be concluded that waves with higher water depth is difficult to reach liquefaction.

Both of Figs. 6 and 7 can be explained combining the influence of currents on wave patterns which has been discussed in the last paragraph. Here list three ways which could possibly lead to the wave steepness (H/L)'s increase: (1) when waves travelling against currents which can be
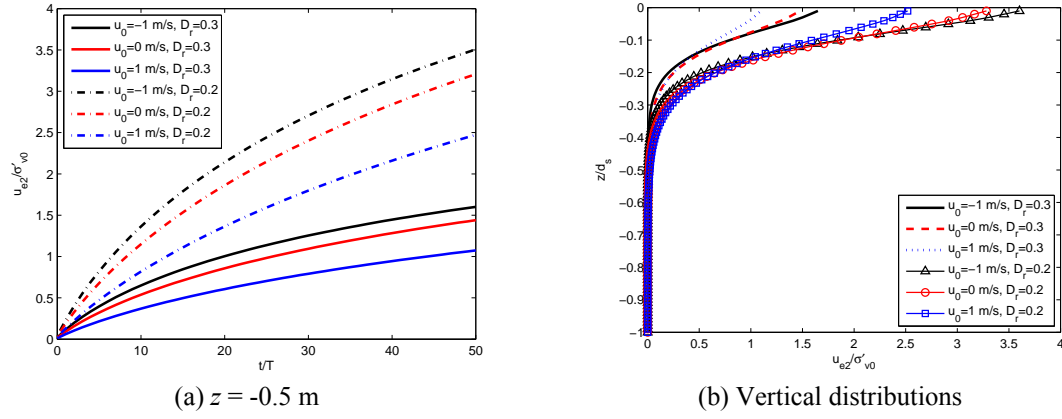
(a) z = -0.5 m

(b) Vertical distributions

Fig. 8 Pore pressure accumulation with various current velocities and relative density at $t/T = 50$
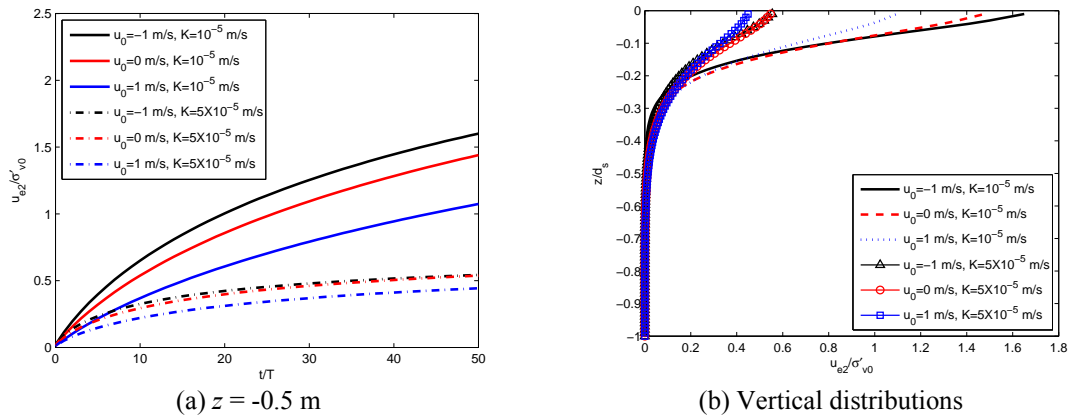

(a) z = -0.5 m

(b) Vertical distributions

Fig. 9 Pore pressure accumulation with various current velocities and soil permeability at $t/T = 50$

found in Fig. 4; (2) the decrease in water depth for which results in the decrease in wave length; and (3) the increase in wave height itself. When the wave steepness increases, the water pressure fluctuations could penetrate into deeper locations. As a result, the pore pressure accumulation process is more likely to be happen in the cases of higher wave height and shallower water depth as well as the case when waves travelling against currents.

4.3 Effect of soil properties on seabed response

It can be found in the residual soil response section that the parameter *Dr* and soil permeability *K* play an important role in the pore pressure accumulation process. As is well known, *Dr* is relevant to soil void ratio and *K* related to the drainage level of the soil, since the buildup occurs normally in soils with low permeability. It is more difficult for a soil with higher *Dr* or higher permeability to arrive liquefaction as shown in Fig. 8 and Fig. 9. Besides, it is easy to find that there is totally no liquefaction occurs in the case of $K = 5 \times 10^{-5}$ m/s at $t/T = 50$ (Fig. 9(b)). That is due to the fact that the pore pressure would be relieved when fluid could easily "escape" from the

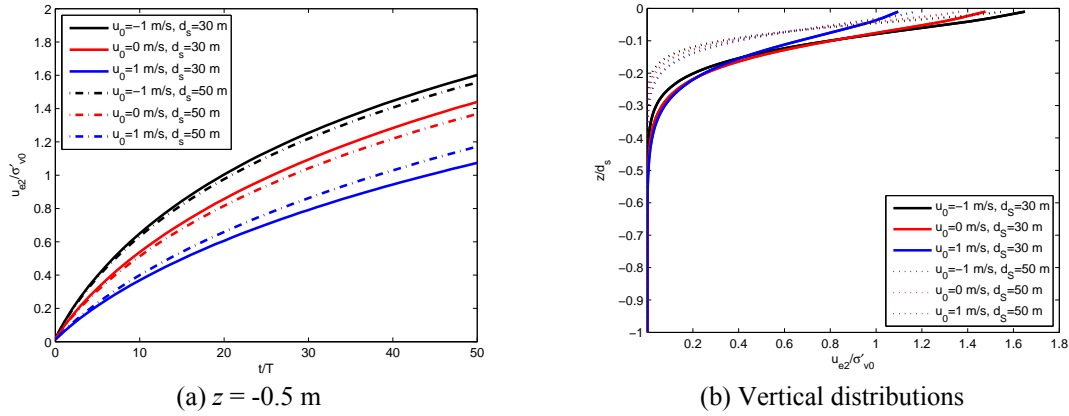(a) $z = -0.5$ m   (b) Vertical distributions

Fig. 10 Pore pressure accumulation with various current velocities and seabed thickness at $t/T = 50$

space among soil grains (Sumer and Fredsøe 2002). Therefore no build-up of pore pressures would happen in this case.

Besides these two important seabed parameters (relative density of soil and soil permeability) we discussed, soil thickness is another factor, which should be taken into account. The pore pressure accumulation processes under two different seabed thicknesses as well as different current velocities are illustrated in Fig. 10. It seems that the value of u_{e2}/σ'_{vo} changes faster along the vertical direction for deeper seabed compared to shallower one (Fig. 10(b)), but it has a slight influence on the seabed pore pressure accumulation process (Fig. 10(a)) compared to other soil parameters.

4.4 Development of liquefaction zones

With the present poro-elastic soil model, the development of liquefaction zone could be fully examined. According to Sassa and Sekiguchi (1999), the liquefaction took place when the accumulated pore pressure reaches the value of the initial vertical effective stress

$$u_{e2} = \sigma'_{v0}(z) \tag{22}$$

By applying this liquefaction criterion, the development of liquefaction zone for the case $u_o = 0$ m/s can be plotted in Fig. 11. As is shown in Fig. 11, the liquefaction zone appears to be a two-dimensional pattern at the 25th wave cycle, as the following of progressive waves, it gradually changes to a one dimension case. It can also be better explained by Fig. 12 which demonstrates the pore pressure accumulation process at three different location - (110, -0.2), (118, -0.2) and (127, -0.2) along the *x*-direction. In general, the trends of pore pressure accumulation for these cases are almost the same as shown in Fig. 12(a), but the amplified figure – Fig. 12(b) reveals that the speeds of pore pressure accumulation at (110, -0.2) and (127, -0.2) are almost the same and fast than at (118, -0.2). This phenomenon implies that the former two locations would reaches its liquefaction status at first, then when liquefaction happens at (118, -0.2), the liquefaction zone would transfer to a line, that's why the liquefaction zone would change from the two dimensional pattern to one dimensional pattern.
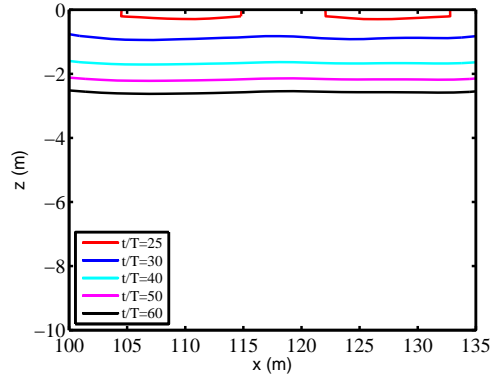
Fig. 11 The histories of development of liquefaction zone for the case of $u_o = 0$ m/s
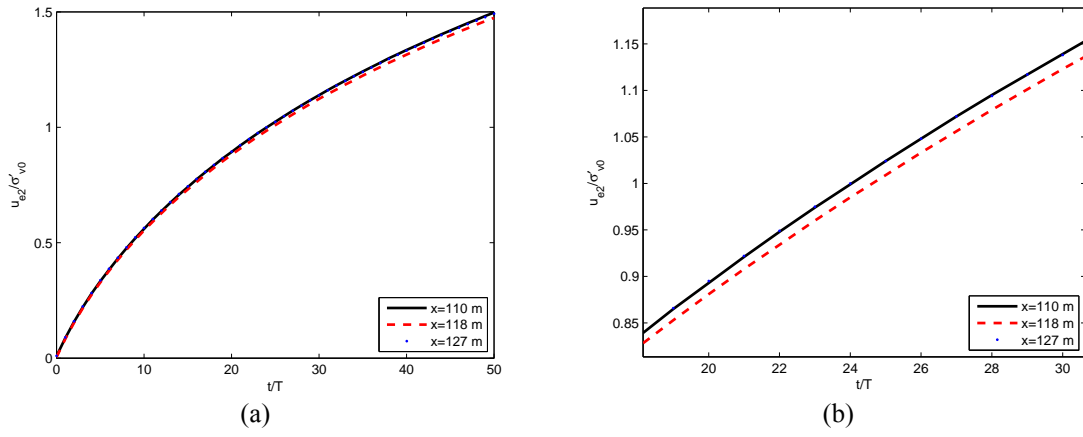

(a)   (b)

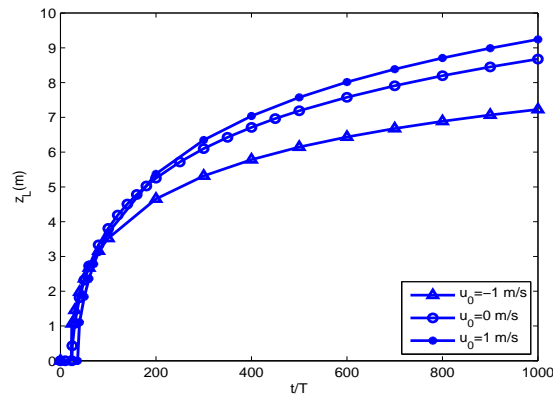Fig. 12 Pore pressure accumulations along *x*-direction at $z = -0.2$ m for the case of $u_o = 0$ m/s

Fig. 13 The development of liquefaction depth under different current velocities

On the other hand, it can be easy found from Fig. 11 that the speed of liquefaction zone development becomes slower and slower as time goes by. It can be better understood through a diagram of liquefaction depth development versus time. In Fig. 13, the liquefaction depths under different current velocities are plotted. It can be seen from the figure that the liquefaction depth increases fast during the former 50 wave periods for all cases, the development for all the cases are almost the same with a little more fast speed for the case of $u_o = -1$ m/s. However, great distinctions come out after t/T around 200. The line which stands for the case of $u_o = 1$ m/s shows a deeper potential of its liquefaction depth compared to the other cases, and the case of $u_o = -1$ m/s owns a shallowest liquefaction depth during 1000 wave periods.

5. Conclusions

In this study, a two-dimensional integrated model with wave-current model and poro-elastic soil model is presented. The model is validated first and then applied to simulation of the seabed response under combined waves and currents. Based on the results obtained from the simulation, it can be concluded that:

- The existence of current leads to a great discrepancy to the fluid field as well as seabed soil response. When waves travel against the currents, it results in a decrease in wavelength and an increase in wave height. On contrary, when waves travel following the currents, the wavelength increases and the wave height reduces. It also found that waves with opposite currents reach its liquefaction status faster than waves with following currents, and the case of no current falls in between.
- Both wave parameters and soil parameters could result in a great influence on seabed response. Higher wave height and shallower water depth leads to faster liquefaction development; higher relative density and higher permeability makes the soil difficult to liquefy; seabed thickness has little influence on the seabed response compared to other parameters.
- Along the seabed surface, a portion of soil grains reach its liquefaction status first and then the remaining. As a result, the liquefaction zone behaves from a two dimensional pattern to one dimensional pattern under progressive waves.
- Differences among current velocities results in great disparities of the liquefaction depth. It can be concluded that waves with following currents have a deeper liquefaction depth compared to the waves only case, waves with opposite currents have a shallowest liquefaction depth.

Acknowledgments

References

Biot, M.A. (1941), "General theory of three-dimensional consolidation", *J. Appl. Phys.*, **26**(2), 155-164.
Biot, M.A. (1956), "Theory of propagation of elastic waves in a fluid-saturated porous solid, Part I: Low

frequency range", *J. Acoust. Soc., Am*., **28**(2), 168-178.

Grant, W.D. and Madsen, O.S. (1979), "Combined wave and current interaction with a rough bottom", *J. Geophys. Res*., **84**(C4), 1797-1808.

Hirt, C.W. and Nichols, B.D. (1981), "Volume of fluid(VOF) method for the dynamics of free boundaries", *J. Comput. Phys*., **39**(1), 201-225.

Hsu, H.C., Chen, Y.Y., Hsu, J.R.C. and Tseng, W.J. (2009), "Nonlinear water waves on uniform current in Lagrangian coordinates", *J. Nonlinear Math. Phys*., **16**(1), 47-61.

Israeli, M. and Orszag, S.A. (1981), "Approximation of radiation boundary conditions", *J. Computat. Phys*., **41**(1), 115-131.

Jeng, D.S. (2013), *Porous Models for Wave-seabed Interactions*, Springer.

Jeng, D.S. and Ou, J. (2010), "3D models for wave-induced pore pressure near breakwater heads", *Acta Mechanica*, **215**(1), 85-104.

Jeng, D.S. and Seymour, B.R. (2007), "A simplified analytical approximation for pore-water pressure build-up in a porous seabed", *J. Waterw Port Coast. Ocean Eng*., **133**(4), 309-312.

Kemp, P.H. and Simons, R.R. (1982), "The interaction of waves and a turbulent current: Waves propagating with the current", *J. Fuild Mech*., **116**, 227-250.

Kemp, P.H. and Simons, R.R. (1983), "The interaction of waves and a turbulent current: Waves propagating against the current", *J. Fuild Mech*., **130**, 73-89.

Launder, B.E. and Spalding, D.B. (1974), "The numerical computation of turbulence flows", *Comput. Method. Appl. Mech. Eng*., **3**(2), 269-289.

Li, T., Troch, P. and Rouck, J.D. (2007), "Interactions of breaking waves with a current over cut cells", *J. Comput. Phys*., **223**(2), 865-897.

Liao, C.C., Zhao, H.-Y. and Jeng, D.-S. (2014), "Poro-elastoplastic model for wave-induced liquefaction", *Proceedings of the 33rd International Conference on Ocean, Offshore and Arctic Engineering* (*OMAE2014*), San Francisco, CA, USA, June. (CD-ROM)

Liao, C.C., Jeng, D.-S. and Zhang L.L. (2015), "Analytical approximation fr dynamic soil response of a porous seabed under combined wave and current loading", *J. Coast. Res*., **31**(5), 1120-1128. DOI: 10.2112/JCOASTRES-D-13-00120-.1

Lin, P. and Liu, P.L.-F. (1999), "Internal wave-maker for Navier-Stokes equations models", *J. Waterw Port Coast. Ocean Eng*., *ASCE*, **125**(4), 207-215.

Liu, B., Jeng, D.-S. and Zhang, J.-S. (2014), "Dynamic response of a porous seabed of finite depth due to combined wave and current loading: Inertial forces", *J. Coast. Res*., **30**(4), 765-776.

Markus, D., Hojjat, M., Wuechner, R. and Bletzinger, K.U. (2013), "A CFD approach to modelling wave-current interaction", *Int. J. Offshore Polaer Eng*., **23**(1), 29-32.

Park, J.C., Kim, M.H. and Miyata, H. (2001), "Three dimensional numerical wave tank simulations on fully nonlinear wave-current-body interactions", *J. Mar. Sci. Technol*., **6**(2), 70-82.

Qi, W.G. and Gao, F.P. (2014), "Water flume modelling of dynamic responses of sandy seabed under the action of combined waves and current: Turbulent boundary layer and pore-water pressure", *Proceedings of the 8th International Conference on Physical Modelling in Geotechnics* (*ICPMG2014*), Perth, Australia, January.

Rodi, W. (1993), *Turbulence Models and their Application in Hydraulics-state-of-the Art Review*, (3rd edition), Balkema, Rotterdam, The Netherlands.

Sassa, S. and Sekiguchi, H. (1999), "Wave induced liquefaction of beds of sand in a centrifuge", *Géotechnique*, **49**(5), 621-638.

Sassa, S., Sekiguchi, H. and Miyamamot, J. (2001), "Analysis of progressive liquefaction as moving boundary problem", *Géotechnique*, **51**(10), 847-857.

Seed, H.B. and Lee, K.L. (1966), "Liquefaction of saturated sands during cyclic loading", *J. Soil Mech. Found. Div.*, *Proceedings of the American Society of Civil Engineers*, **92**(6), 1249-1273.

Seed, H.B. and Rahman, M.S. (1978), "Wave-induced pore pressure in relation to ocean floor stability of cohesionless soils", *Marine Geotechnol.*, **3**(2), 123-150.

Sekiguchi, H., Kita, K. and Okamoto, O. (1995), "Response of poro-elastoplastic beds to standing waves",

Soil. Found., **35**(3), 31-42.

Sumer, B.M. and Cheng, N.S. (1999), "A random-walk model for pore pressure accumulation in marine soils", *Proceedings of the 9th International Offshore and Polar Engineering Conference* (*ISOPE99*), Brest, France, May-June, **1**, 521-528.

Sumer, B.M. and Fredsøe, J. (2002), *The Mechanism of Scour in the Marine Environment*, World Scientific, NJ, USA.

Sumer, B.M., Kirca, V.S.O. and Fredsøe, J. (2012), "Experimental validation of a mathematical model for seabed liquefaction under waves", *Int. J. Offshore Polar Eng.*, **22**(2), 133-141.

Umeyama, M. (2009), "Changes in turbulent flow structure under combined wave-current motions", *J. Waterw Port Coast. Ocean Eng.*, **135**(5), 213-227.

Wolf, J. and Prandle, D. (1999), "Some observations of wave-current interaction", *Coast. Eng.*, **37**, 471-485.

Yamamoto, T., Koning, H., Sellmeijer, H. and Hijum, E.V. (1978), "On the response of a poro-elastic bed to water waves", *J. Fluid Mech.*, **87**(1), 193-206.

Ye, J. and Jeng, D.-S. (2012), "Response of seabed to natural loading-wave and currents", *J. Eng. Mech.*, *ASCE*, **138**(6), 601-613.

Ye, J., Jeng, D.-S., Wang, R. and Zhu, C. (2013), "Validation of a 2-D semi-coupled numerical model for fluids-structure-seabed interactions", *J. Fluid. Struct.*, **42**, 333-357.

Ye, J., Jeng, D.-S., Wang, R. and Zhu, C. (2014), "Numerical simulation of the wave-induced dynamic response of poro-elastoplastic seabed foundations and a composite breakwater", *Appl. Math. Model.*, **39**(1), 322-347.

You, Z.J. (1994), "A simple model for current velocity profiles in combined wave-current flows", *Coast. Eng.*, **23**(3-4), 289-304.

Zen, K. and Yamazaki, H. (1990), "Mechanism of wave-induced liquefaction and densification in seabed", *Soil. Found.*, **30**(4), 90-104.

Zhang, Y., Jeng, D.-S., Gao, F.P. and Zhang, J.-S. (2013a), "An analytical solution for response of a porous seabed to combined wave and current loading", *Ocean Eng.*, **57**, 240-247.

Zhang, J.-S., Zhang, Y., Zhang, C. and Jeng, D.-S. (2013b), "Numerical modeling of seabed response to the combined wave-current loading", *J. Offshore Mech. Arct. Eng.*, *ASME*, **135**(3), 031102.

Zienkiewicz, O.C., Chang, C.T. and Bettess, P. (1980), "Drained, undrained, consolidating and dynamic behaviour assumptions in soils", *Géotechnique*, **30**(4), 385-395.

CC